

## Calibration of CCD cameras for field and frame capture modes

**Mark R. Shortis**

Department of Geomatics  
The University of Melbourne  
Parkville, Victoria 3052, AUSTRALIA  
Telephone : +61 3 9344 6401  
Facsimile : +61 3 9347 2916  
M.Shortis@unimelb.edu.au

**Walter L. Snow**

Experimental Testing and Techniques Division  
NASA Langley Research Center  
Hampton, Virginia 23665, U.S.A.  
Telephone : +1 804 864 4613  
Facsimile : +1 804 864 7607  
W.L.Snow@larc.nasa.gov

**Keywords** : Calibration, CCD, Frame capture, Field capture, Sensor geometry

### ABSTRACT

Small format, medium resolution CCD cameras are at present widely used for industrial metrology applications because they are readily available and relatively inexpensive. The calibration of CCD cameras is necessary in order to characterise the geometry of the sensors and lenses. In cases where a static or slowly moving object is to be imaged, frame capture mode is most often used to maximise the resolution of the CCD sensor. In cases where the object to be imaged is in rapid motion, field mode capture is frequently adopted to avoid discontinuities caused by the interlaced scanning process used by the sensors. A strategy for the computation of calibration parameters for field modes, based on a frame mode calibration, is proposed. The strategy is then verified by testing using real data from test range calibrations of three different types of CCD camera. The results of these calibration tests will be described, with particular emphasis on the changes required to adjust between frame and field capture modes.

### 1. INTRODUCTION

Since their introduction in the 1970s, CCD cameras and digital images have gained wide acceptance for machine vision and industrial metrology. CCD cameras are inexpensive, readily available and offer a wide variety of format, resolution, sensitivity and interface. Digital images are easily captured, stored, manipulated and analysed. Moreover, CCDs are geometrically stable sensors which allow the possibility of reliable and accurate measurement and are relatively immune to environmental effects. The further benefit of video rates of image acquisition allows the possibility of real time vision systems for the recording of dynamic events, such as tracking an object in free flight or monitoring a production line system. Both qualitative and quantitative applications of machine vision are widespread in the manufacturing, aerospace and automobile industries. The breadth of the metric, quantitative applications has given rise to a relatively new science, variously known as vision metrology, videometrics or digital photogrammetry.

CCD cameras are treated as a central projection system in the same way that traditional film cameras are used for photogrammetry. However, the major difference with CCD cameras is the small format size. Whereas some photogrammetric cameras have formats of up to 230 mm by 230 mm, the largest commercially available CCD sensors have formats of the order of 30 mm by 30 mm. The reduction in effective resolution is partly compensated by digital image processing techniques, but CCD sensors are, at least for the present, somewhat limited in their theoretical accuracy as compared to conventional film cameras.

Whilst there are clear differences in the characteristics of videometric and photogrammetric cameras, calibration has been and will always be a necessary part of the measurement process. Knowledge of the internal geometry of the camera is essential if the principle of collinearity is to be correctly applied. Without this knowledge, derived measurements in the object space will be affected by systematic errors and therefore will be degraded in accuracy. It is generally accepted and has been widely demonstrated that self-calibration is the most accurate method of modelling the systematic errors in the camera imaging system. Self-calibration has the substantial advantage that the calibration is carried out simultaneously with the measurement of the object of interest, and the calibration therefore corresponds directly with the prevailing camera configuration at the time of the photography or imagery.

In many circumstances self-calibration of CCD cameras may be feasible, but in many cases such an approach is not appropriate. Self-calibration is typically ruled out because the geometry of the photogrammetric network is too weak to determine the calibration parameters with confidence or with a reasonable degree of independence. The internal characteristics of the camera must therefore be determined before or after the actual measurement process, or preferably both. The very nature of the tasks in which CCD cameras are employed tends to exacerbate rather than ameliorate the

calibration problem. Real time or near real time applications require multiple, fixed (and synchronised) cameras (El-Hakim, 1992; Haggrén and Leikas, 1987; Maas, 1991), whereas self-calibration is most effective with a single, portable camera (Fraser and Shortis, 1995). Further, such applications often involve small numbers of targets, whereas a dense, three dimensional array of targets which fills the camera format vastly increases the effectiveness of self-calibration.

## 2. DYNAMIC TRACKING APPLICATIONS

Dynamic situations introduce a further complication into the calibration and utilisation of CCD cameras. The majority of off-the-shelf CCD cameras produce interlaced images, a legacy of the low transmission bandwidth of early television broadcast systems. The full frame of each image is broken up into two fields of even and odd horizontal scan lines which are recorded and transmitted separately (see Figure 4). This has the benefit of reducing the required transmission speed without significant visual impact. Furthermore, for metric applications with static objects there is no disadvantage when interlaced images are acquired.

However, the quantitative analysis of interlaced images has the distinct disadvantage that dynamic objects are displaced between the even and odd scans. Figure 1 shows an image acquired during a recent application of CCD cameras to characterise the motion of a free-flight model in a large wind tunnel at NASA Langley Research Center (Childers et al, 1994). The intent of the project was to determine the proximity of the model to a generated vortex core, in order to characterise the effect on the aircraft flight path and attitude. Nine retro-reflective targets were tracked by two synchronised CCD cameras to derive the 6 degrees of freedom of the model from recorded image sequences. The results are presented as graphs of position and orientation with respect to time.

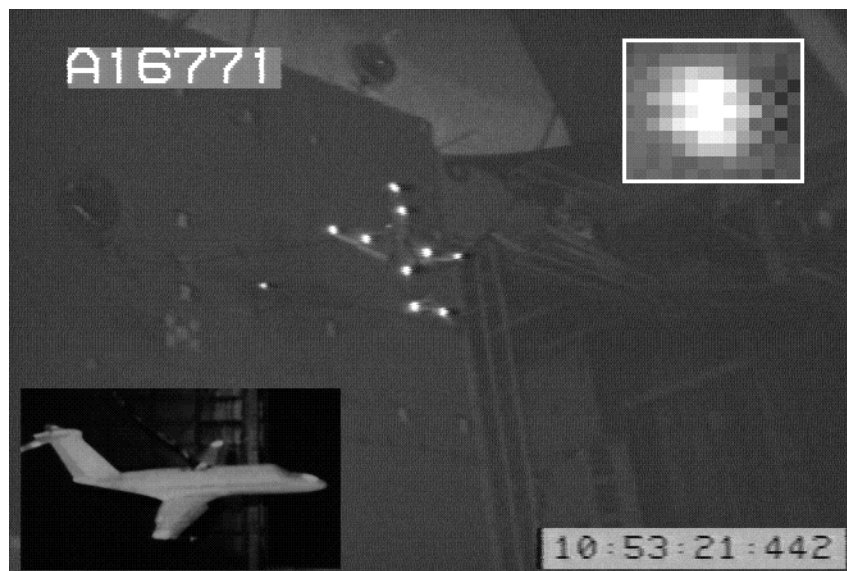


Figure 1. Full frame CCD camera image of a free flight model with (inset lower) the actual model and (inset upper) the effect of motion on one of the retro-targets.

The full frame shows no impairment of the image at first glance, confirming the previous supposition that the visual impact of motion can be minimal. However, the inset image in Figure 1 clearly shows the displacement of one of the retro-reflective targets due to the movement of the model during the time between the interlaced scans. In this case the displacement is not catastrophic, as the motion of the model was relatively small in magnitude. This displacement was essentially ignored and full frames were analysed to determine the 6 degrees of freedom.

It is arguable whether the free flight model application would have drawn any overall benefit from changing the analysis from full frames to fields. Fields are acquired at twice the rate of frames, typically at 60Hz as opposed to 30Hz frequency. Therefore the movement can be tracked with less subsequent interpolation in time or position, and the scan line displacement problem is circumvented. On the other hand, the vertical resolution of the fields is half that of the full frame. Consequently, the amount of data available to track each retro-reflective target is halved, weakening the accuracy of the centroid computation used to determine the image location (Trinder, 1989). But perhaps the critical factor in this case was that the amount of data acquisition, measurement and analysis would have been doubled, and the doubling of time and resources required was not warranted given the small displacements.

Fast motion does demand the highest sample rate available from the video imagery. Without resorting to specialised, high speed video systems, the 60Hz field rate is the obvious choice to minimise interpolation between samples. The use of field capture has been adopted for applications such as human movement studies (Baltsavias and Stallman, 1992). The principle will be illustrated here with a second application of model tracking in a wind tunnel at Langley. The 20 foot vertical spin tunnel at Langley is used to characterise the motion of aircraft models during a vertical spin and spin recovery (Snow et al, 1992). Once more, the location of retro-reflective targets imaged by synchronised CCD cameras are used to derive the 6 degrees of freedom of the model. The results are presented as graphs of position change and rate of spin with respect to time.

Figure 2 shows a full frame from one of the cameras in the spin tunnel. The full frame does show impairment of the image and the inset on the lower right confirms catastrophic displacement of the retro-target between field scans. It is unlikely that the location of such a target could be measured accurately, if at all, by a centroid or any similar location algorithm.



Figure 2. Full frame CCD camera image of a spin tunnel model with (inset upper) the actual model and (inset lower) the effect of motion on one of the retro-reflective targets.

Figure 3 shows a sequence of six fields which demonstrates the typical motion of the model. The clearly identifiable shifts and rotations between consecutive fields confirms that the processing of fields is desirable for the application. Whilst the 60Hz sample rate was deemed adequate to characterise the spin of the model, faster rates would guarantee an accurate delineation of the motion. As previously mentioned, high speed cameras and/or video tape systems are available with rates as high as 15kHz (Maas, 1992), but the cost of purchase or hire of such systems is much greater than off-the-shelf CCD cameras and video tape systems and the resolution may be considerably less than off-the shelf CCD sensors. A further disadvantage of high speed video systems is that, in general, they require special interfaces which are not compatible with off-the-shelf video systems. This often leads to difficulties when acquiring or analysing such images with systems set up for standard video input.

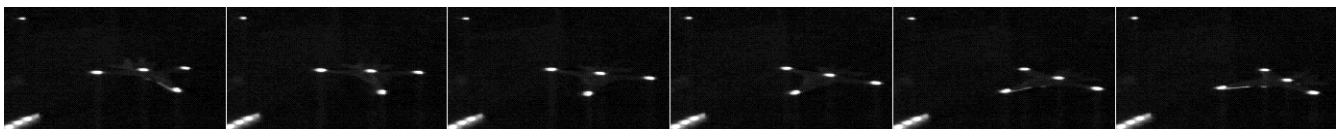


Figure 3. A sequence of 6 consecutive fields of a spinning model (shown in Figure 2) acquired from one of the CCD cameras in the spin tunnel : the bank of lights and fixed retro-target at the left of each frame are included to provide a reference.

The issue to be resolved for field recording is the calibration of the cameras. Typically, cameras are pre- or post-calibrated in the configuration which will be used for the actual measurement. The configuration includes such aspects as temperature, recording method, synchronisation and certainly the image acquisition mode. However this implies that any single camera must be calibrated three times to obtain a comprehensive knowledge of the calibration for frame acquisition, even field acquisition and odd field acquisition. Once this calibration information is obtained, the internal characteristics would then have to be applied specifically to each image acquisition mode.

Notwithstanding the logic of the previous discussion, there are a number of common calibration parameters regardless of the image acquisition method. The focal length and lens distortions of the camera will not change. The principal point location in the horizontal scan line direction and the affinity, if present, of the sensor and/or the frame grabber will not change. As will be shown in the next section, the only parameters which do change are the vertical spacing of the horizontal scan lines and the location of the principal point in the vertical scan direction. It therefore seems logical to carry out a single calibration in frame acquisition mode and apply the two changes to convert to field recording mode. The intent of this paper is to define the differences in calibration parameters and calibration accuracy between the different image acquisition modes. The theoretical differences will be derived in the next section. The theory will then be verified by laboratory tests of a representative sample of cameras and target images.

### 3. FRAME VERSUS FIELD RECORDING

The geometry of a full frame of a digital image acquired from an interlaced video source is shown at the top of Figure 4. The even and odd scan lines are shown in their actual relationship on the CCD sensor or, equally, after they have been re-assembled into a full frame by the acquisition device. The vertical spacing of the scan lines is equivalent to the vertical separation of the pixel sites on the sensor. The horizontal spacing of the image pixels is equivalent to the horizontal spacing of the pixel sites on the sensor (or as translated by the frame grabber if the horizontal frequencies of the sensor and grabber are incompatible). The horizontal pixel spacing, horizontal retrace and vertical retrace are not shown in the figure for reasons of clarity.

The horizontal and vertical structure of the pixels and the scan direction provides an implicit coordinate system in terms of rows and columns, with the origin at the upper left. This dimensionless system is most often used for non-videometric storage, manipulation and communication of digital images. For videometric purposes, an image coordinate system is adopted at the centre of frame with the x-y system corresponding to the photogrammetric convention for image coordinates. The initial position for the centre of frame is simply adopted as the half way point in each direction. Coordinates are typically quoted in millimetres, based on the pixel spacing specified for the sensor. Hence, there is a simple conversion from pixel coordinates to image coordinates :

$$x = \text{column} * s_h - x_c \qquad y = y_c - \text{row} * s_v \qquad (1)$$

and 
$$x_c = 0.5 * s_h * n_h \qquad y_c = 0.5 * s_v * n_v \qquad (2)$$

where  $s_h, s_v =$  spacing of horizontal and vertical pixels for the sensor  
 $x_c, y_c =$  centre of frame coordinates  
 $n_h, n_v =$  numbers of horizontal and vertical pixels for the sensor

For consistency with the mechanisms by which images are handled for non-videometric purposes, the storage of fields is analogous to that for full frames. There are two obvious consequences, viz the image storage and the number of rows are both halved. To reconcile this storage method with the physical layout on the CCD sensor, field images must adopt the geometric layout shown at the bottom of Figure 4. To cover the vertical extent of the sensor, the vertical spacing of the scan lines is doubled. The odd field commences with the zero scan line slightly displaced to accord with the start of the scan on the sensor.

From inspection of Figure 4, for the even field it is clear formulae (1) and (2) can be applied without change, given that the vertical spacing is doubled and the row count is halved. For the odd field there must be a constant correction to the y coordinates because of the offset at the start of the scan. However, rather than change the basic pixel to image coordinate conversion process, it is more convenient to alter the principal point offset as part of the camera calibration. The y component of the principal point should be increased by one standard pixel spacing for the odd field to obtain an equivalent coordinate to that of the full frame.

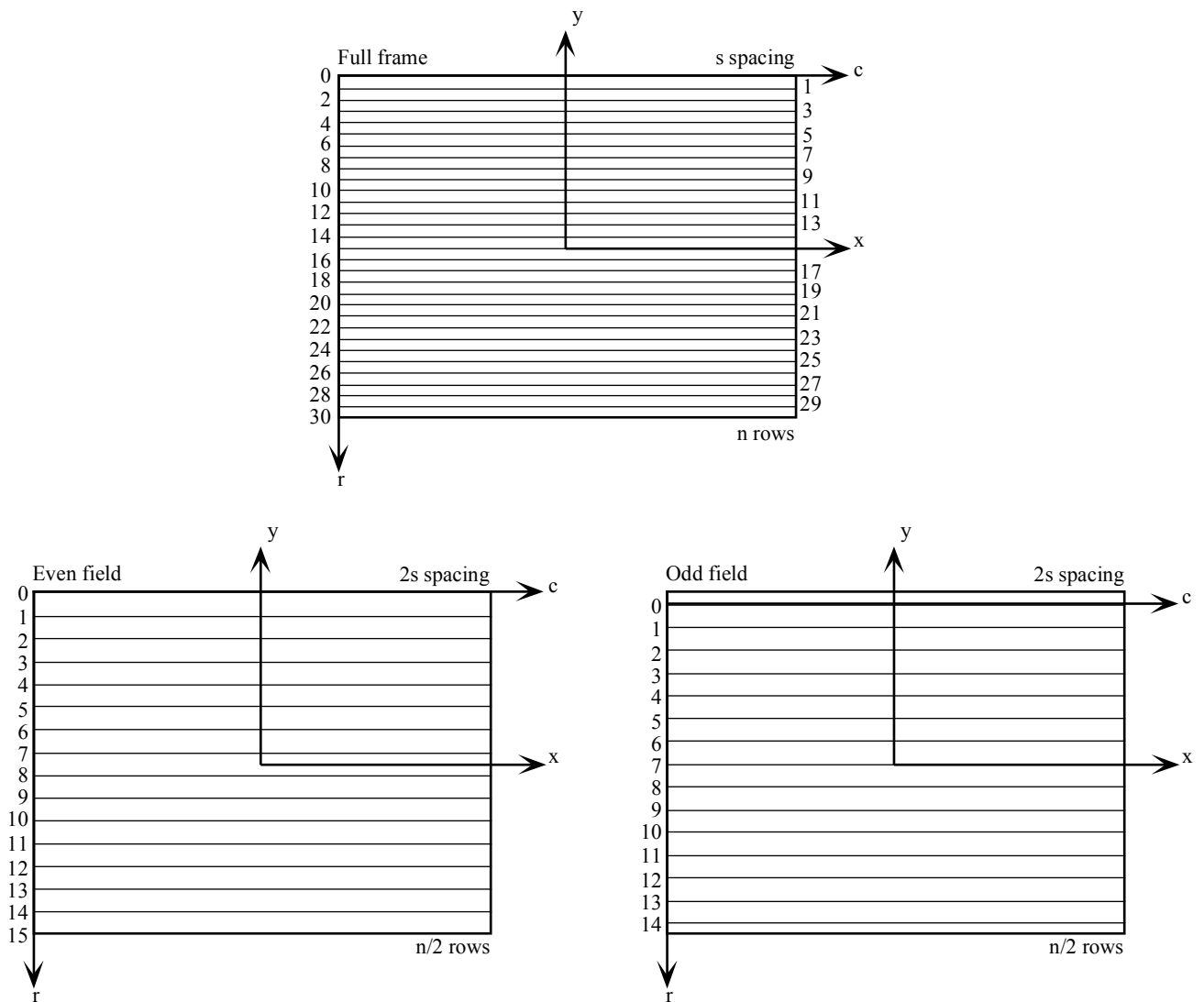


Figure 4. Geometry of a full frame (top) and the even and odd fields (bottom) of an interlaced digital image.

The reason for this strategy is that a further correction of the principal point position must be made due to the mechanism by which discrete targets are imaged. Figure 5 shows how a selection of binarised target images are broken up when the full frame is deconstructed into the even and odd fields. In the limited number of cases of approximately circular targets shown in Figure 5 it is apparent that many of the centroids of the target images will be displaced on the even and odd fields, because of the reduced samples of the image obtained by the interlaced scan. The magnitude of the displacement is dependent on the size of the image and the location of the image. Careful analysis of many cases indicates that the mean displacement of a discrete target image is one half of the standard full frame pixel spacing toward the bottom of frame. This result is independent of the target image size and is logical from the adopted scheme of double spacing of the even and odd fields.

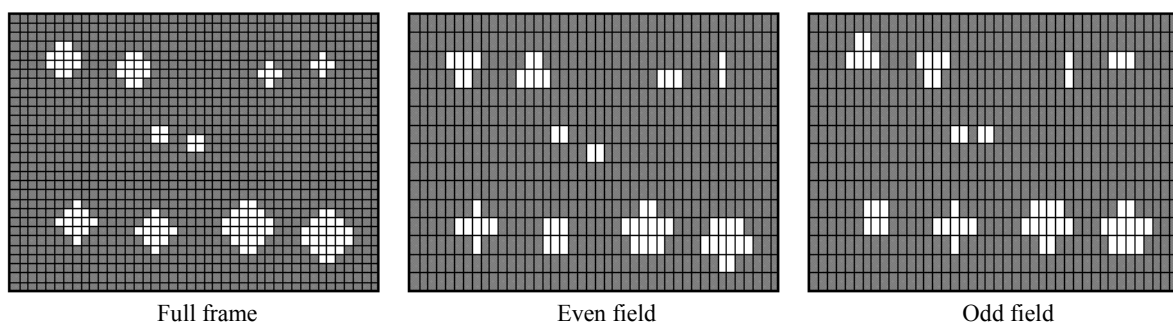


Figure 5. Deconstruction of an interlaced full frame of binary target images into the even and odd fields.

Again, rather than changing the computation scheme for different field types, it is more convenient to alter the y component of the principal point position to compensate for the above effects. The even field principal point should be decreased by one half of a pixel spacing, whilst the odd field principal point y location should be increased by one half of a pixel spacing. The adjustment for the odd field is a combination of the geometry correction and the mean target displacement. All other components of the camera calibrations for the fields should be unchanged from that of the full frame images.

A less obvious consequence from the case by case analysis above is that a pseudo-random error is introduced into the target image positions. Even and odd field centroids have a opposite displacements of varying magnitude, compared to the full frame image. The pseudo-randomness is caused by the random sizes and positions of the target images on a real frame. For centroids of approximately circular binary images, the root mean square (RMS) error of target image locations for the even and odd field images, as compared to the full frame image, is 0.11 pixels. Again, this is a logical consequence from the interlaced scanning, and is especially evident in Figure 5 for target images which span an even number of pixels greater than two. Surprisingly, this result is independent of the size of the target image, for a binary image.

The analysis for grey scale images is more complex due to the large number of cases which would need to be analysed to confidently predict a result. Hence a thorough theoretical analysis is necessary, which is beyond the scope of this paper. Analysis of a small number of cases indicates, as could be intuitively expected, that the RMS will reduce with an increase in diameter of the target images. This effect can be attributed to the greater weight of the high intensity, central pixels in the calculation of the weighted centroid.

The analysis for small target images becomes less certain. Target images spanning one pixel will of course disappear from one field, and the RMS error for target images spanning two pixels is proportionately very large at 0.5 pixels. Very small target image diameters are generally avoided as the accuracy of centroid locations degrades rapidly (Trinder, 1989). For accurate measurement, maintaining target image diameters greater than a few pixels assumes even greater importance for the analysis of images acquired as fields. However the physical size of targets always has a finite limit, enforced by the size of the object to be tracked, field of view versus motion envelope considerations, and the environment of the application (see Figures 1 and 2).

#### 4. LABORATORY TESTING

##### 4.1 CCD Camera Characteristics

To verify the effects on field images predicted in the previous section, a number of CCD camera calibrations reported previously (Shortis et al, 1995) were re-analysed. A small routine was written to split the full frame images into even and odd fields so that the calibrations of the three types of images could be compared. Three cameras were chosen as a representative sample from the eleven cameras originally calibrated. The principle difference between the camera specifications (shown in Table 1) are the resolutions of the sensors. The Hitachi camera is the obvious candidate as an off-the-shelf sensor which outputs an interlaced signal appropriate for 60Hz analysis. The two scientific sensors are certainly not capable of this type of output, as they are both slow-scan read out systems. They are included here purely to test the influence of large target images on the calibration results. The calibration set up (see below) was so arranged that the higher resolution sensors imaged proportionally larger target images. To equalise the radiometric resolutions, the images for the Kodak KAF 1400 sensor were compressed from 4096 to 256 grey levels.

CCD Camera	Sensor Type	Grey Level Range	Horizontal Pixels	Vertical Pixels	Horizontal Spacing (um)	Vertical Spacing (um)	Focal Length (mm)
Hitachi KP-M1	2/3" interline	256	752	480	11.0	13.0	12.5
Kodak KAF 1400	Scientific	4096	1320	1034	6.8	6.8	24
Kodak 4.2 Megaplus	Scientific	256	2028	2044	9.0	9.0	24

Table 1. Characteristics of the calibrated CCD cameras

## 4.2 Calibration Technique

The requirement for pre- and/or post-calibration of CCD cameras at Langley is a direct result of applications such as the wind tunnel testing previously described. The placement of cameras and target arrays is severely limited within the test zones of wind tunnels and self-calibration is rarely possible due to the constraints on network geometry. Pre- or post-calibration is routinely carried out at Langley using one of a number of established test fields. The test fields are two or three dimensional arrays of suitable targets, generally with known coordinates from an independent measurement process, such as a coordinate measuring machine. However, known target coordinates are not necessary. If the geometry of the photogrammetric network is well designed (Shortis and Hall, 1989) and only the primary physical calibration parameters (principal point, principal distance, lens distortions, image orthogonality and image affinity) are desired then the situation reverts to a self-calibration. The calibration is in effect taking advantage of a better network geometry which can not be obtained during operational photography within the wind tunnel environments. In order to confidently derive the calibration parameters, the geometry of the network should be essentially the same as that required for self-calibration. Multiple, convergent images of the target field are acquired, preferably with a range of camera to object distances and a variety of roll angles to reduce correlations between parameters. The use of target fields to calibrate CCD cameras has been successfully implemented by a number of researchers (Beyer, 1987; Bösemann et al, 1990; Gustafson and Handley, 1992; Wiley and Wong, 1995).

Self-calibration of CCD cameras using the targeted test field technique does have potential problems. The small size of the sensor area and the relatively long principal distances give rise to strong correlations between internal and external orientation parameters. Typical of these is the projective coupling between the principal point location, decentring distortion and (for example) the tip and tilt of the camera, as small changes to any of these parameters results in similar changes within the image space. Parameter constraint is the usual remedy, taken to the extreme of parameter suppression in some cases. Because it is rare for two parameters to be 100% correlated there is always some unavoidable degradation of the accuracy from the network adjustment, caused by unmodelled systematic errors.

To reduce the level of correlation internally between the primary physical parameters, and between these parameters and external orientation parameters, an initial plumb line calibration is carried out. This technique was originally developed by Brown (1971) for close range cameras, but has been successfully and routinely applied to aerial (Hentschel and Shortis, 1991), tube type video (Burner et al, 1985) and CCD video cameras (Fryer and Mason, 1989). The technique is capable of deriving the lens distortion parameters independently from all other parameters, and the results of the plumb line calibration are used to constrain the subsequent self-calibration. The combination of the plumb line and targeted test range calibrations produces an accurate set of calibration parameters with a high degree of independence (Shortis et al, 1995).

## 4.3 Data Acquisition and Processing

The calibration set up used within the laboratory is shown in Figure 6. The target field is a black aluminium plate with an array of 121 passive targets, which are a mixture of targets flush with the surface and stand-off targets on rods. Diffuse overhead lighting and passive targets were adopted to avoid the response fall off of retro-reflective targets at high incidence angles. The target field, mounted on a turntable, encloses a volume of 0.5m by 0.5m by 0.25m. Eight frames of the targeted test field were taken with each camera. The geometry of the network adhered to the optimal ring configuration and 90° convergence (see Figure 6) proposed by Fraser (1986). The camera was rolled about the optical axis by 45° after each frame. The camera to object distance was set in each case as a compromise between maximum coverage within the format of the sensor and minimal target image losses at the edge of the frame due to changes in perspective and camera roll. As a consequence, the average target image diameters increase proportionally to the resolution of the CCD sensor. The target images spanned 7, 15 and 30 pixels on average for the Hitachi, Kodak KAF 1400 and Kodak Megaplus 4.2 cameras respectively.

Using the same focus setting and camera to object distance, three or four frames of a plumb line calibration range (in the background of Figure 6) were taken with each camera. The camera was rolled about the optical axis by 45° after each frame. The plumb lines are white plastic cords, under tension, against a black background. The plumb lines were diffusely illuminated using a mixture of overhead and auxiliary lighting. The grey levels were monitored to maximise the target or plumb line signal, and minimise the background, whilst avoiding saturation of the sensor. Pixel intensities in the target field frames averaged 200 and 5 for the target images and the background, respectively. Pixel intensities in the plumb line range frames averaged 150 and 20 for the plumb line images and the background, respectively.

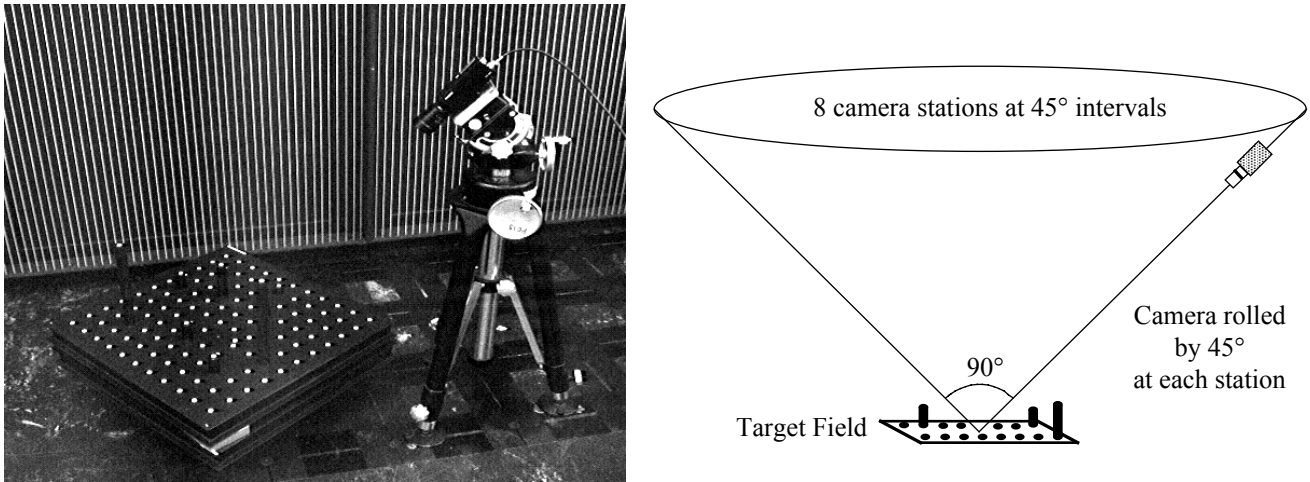


Figure 6. Calibration set up : the target test field and plumb line range (left) and the geometry of the test field network (right).

The target images are located within the frame using a semi-automated procedure based on the known object space coordinates of the targets and a resection/intersection computation (Shortis et al, 1991). Each data set of eight frames comprised approximately 900 target images. Positions on the plumb lines were gathered using a semi-automated procedure based on simple line following. Measurement of each frame produced approximately 20 locations on 20-35 plumb lines, leading to a total ranging between 1500 and 2500 image locations from the four frame sets.

The data from the three CCD cameras for each of the three types of image was processed using the CRAMPA suite of programs (Shortis, 1989) executed on an IBM compatible PC. All plumb line calibration data sets were initially processed using a principal point at the centre of the frame. All target field data sets were then treated as self-calibrating free networks, each with an implicit datum supplied by internal constraints, and explicit constraints supplied by the lens distortion parameters from the plumb line data. The new principal point position was then adopted for the re-computation of the plumb line data set. The target field network was then re-computed as before. The iterative process was then continued until there were no significant changes to the calibration parameters (Shortis et al, 1995).

## 5. ANALYSIS OF RESULTS

Table 2 presents the results of the initial calibrations for the y component of the principal point. The trends in the results for the even and odd fields are clearly correct, yet equally clearly, there remains some significant discrepancies between the predicted and actual results.

Principal Point $y_p$	Full Frame	Even Field			Odd Field		
		Predicted	Actual	Error	Predicted	Actual	Error
CCD Camera	(mm)	(mm)	(mm)	(pixels)	(mm)	(mm)	(pixels)
Hitachi KP-M1	0.2158	0.2093	0.2099	0.05	0.2223	0.2262	0.22
Kodak KAF 1400	-0.0394	-0.0428	-0.0427	0.01	-0.0360	-0.0371	0.16
Kodak 4.2 Megaplus	-0.1020	-0.1065	-0.1041	0.27	-0.0975	-0.0946	0.32

Table 2. Results for the y component of the principal point from the initial network solutions.

An evaluation of the other results of these initial calibrations indicated that the stochastic behaviour of the networks was absorbing part of the signal for the principal point shift. The largest influence on the absorption was the camera station locations. A second set of network solutions were computed with the camera stations for the even and odd field images locked to the positions for the full frames. The results are shown in Table 3 and are confirmation that the predicted shifts in the principal point are correctly modelled. There were no significant changes to any other calibration parameters from the full frame solution to the field solutions.

Principal Point $y_p$	Full Frame	Even Field			Odd Field		
		Predicted (mm)	Actual (mm)	Error (pixels)	Predicted (mm)	Actual (mm)	Error (pixels)
CCD Camera	(mm)						
Hitachi KP-M1	0.2158	0.2093	0.2094	0.01	0.2223	0.2223	0.00
Kodak KAF 1400	-0.0394	-0.0428	-0.0428	0.00	-0.0360	-0.0360	0.00
Kodak 4.2 Megaplus	-0.1020	-0.1065	-0.1065	0.00	-0.0975	-0.0975	0.00

Table 3. Results for the y component of the principal point from the network solutions with locked camera stations.

The comparisons of RMS image residuals from the network solutions for the calibrations are shown in Table 4. The values for the even and odd field image types were computed from networks where both the camera stations and calibration values were locked to those of the full frame images. This strategy was adopted to prevent any absorption of the pseudo-random error by the stochastic nature of the solutions. However, the networks computed for the results shown in Tables 2 and 3 produced results remarkably consistent with those shown in Table 4.

Image Residuals	Full Frame RMS ( $\mu\text{m}$ )	Even Field	Even - Full		Odd Field	Odd - Full	
		RMS ( $\mu\text{m}$ )	Difference ( $\mu\text{m}$ )	Difference (pixels)	RMS ( $\mu\text{m}$ )	Difference ( $\mu\text{m}$ )	Difference (pixels)
CCD Camera							
Hitachi KP-M1	0.33	1.02	0.97	0.07	1.00	0.94	0.07
Kodak KAF 1400	0.21	0.25	0.14	0.02	0.24	0.12	0.02
Kodak 4.2 Megaplus	0.60	0.60	0.00	0.00	0.60	0.00	0.00

Table 4. Results for and differences in the image residuals from the network solutions.

The inflation of the RMS image errors for the field images is evident, as is the expected reduction with increase in the target image diameters. The maximum inflation of 0.11 pixels is not realised for the Hitachi camera, probably for two reasons. First, the seven pixel diameters of the targets in these images is sufficient for the weighting of centroids to reduce the effect of the field displacements. Second, some of the pseudo-random error in the y image coordinate direction will inevitably be redistributed and absorbed by the stochastic model adopted by the network solutions for the calibrations.

There is an insufficient sample of target sizes here to establish an accurate formulation for the trend, however it is reasonably assured that the curve will be of the form shown in Figure 7. Due to the likely absorption of the pseudo-random error the curve for the small target image diameters is very speculative. A comprehensive study of the phenomenon is required to confidently characterise the shape of the curve in this region, but the value of such a study is questionable because small target image diameters should be avoided in practice.

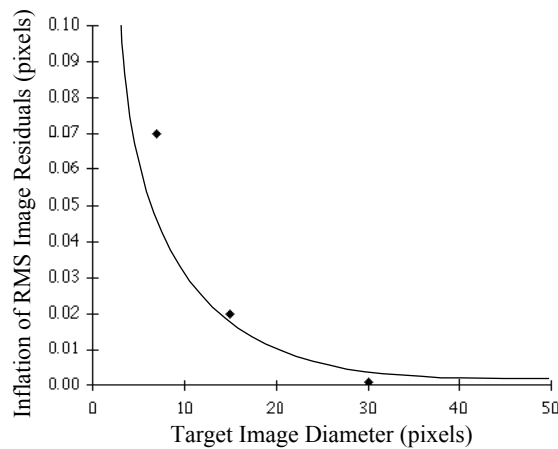


Figure 7. Graph of the approximate inflation of RMS image errors.

## 6. CONCLUSIONS

The theoretical predictions and the analysis of calibrations described in this paper have investigated the relationship between the frame and field image capture modes of CCD cameras. The principle emphasis has been the variations in the calibration due to the change from a full frame to even or odd fields, and the differences in the imaging of discrete targets due to the interlaced scans of the sensor. It has been proven that CCD cameras can be pre- or post-calibrated with full frame images and then, with minor variations, the same calibration parameters can be applied to field mode images. This necessitates only a single calibration of the camera, and allows a consistent conversion process from row and column pixel coordinates to x and y image coordinates.

The prediction and analysis has also revealed and proved that there is a pseudo-random error introduced into the image centroids extracted from field images. The error, caused by displacement of discrete target images within the fields, inflates the RMS image coordinate errors derived from self-calibrating networks. The magnitude of the error is inversely proportional to the target image size. An initial trend curve has been suggested, but more data samples are needed to deduce an accurate relationship between the effect and target image size. However it is clear that large target image diameters are preferable for field mode and this tends to dissipate the effect of the error.

Further research and experimentation outside of the laboratory is necessary to verify the use of the calibration technique for field mode image acquisition. In addition, a greater variety of target image sizes must be analysed so that an accurate relationship between target image size and the pseudo-random error for field recording can be established.

## 7. REFERENCES

- Baltsavias, E. P. and Stallman, D., 1992. Trinocular vision for automatic and robust 3-D determination of trajectories of moving objects. Int. Arch. Photogrammetry and Remote Sensing, Vol. 28(5): 620-629.
- Beyer, H. A., 1987. Some aspects of the geometric calibration of CCD cameras. Proceedings, International Society for Photogrammetry and Remote Sensing Intercommission Conference on the Fast Processing of Photogrammetric Data, Interlaken, Switzerland, pp 68-81.
- Bösemann, W., Godding, R., and Riechmann, W., 1990. Photogrammetric investigation of CCD cameras. Close Range Photogrammetry Meets Machine Vision, SPIE Vol. 1395, pp 119-126.
- Brown, D. C., 1971. Close range camera calibration. Photogrammetric Engineering, 37(8) : 855-866.
- Burner, A. W., Snow, W. L. and Goad, W. K., 1985. Close range photogrammetry with video cameras. Proceedings, Technical Papers, 51st American Society of Photogrammetry Annual Meeting, Washington, U.S.A., pp 62-77.
- Childers, B. A., Snow, W. L., Jones, S. B., Franke, J. M. and Shortis, M. R., 1994. Support of wake vortex detection research in flight and wind tunnel testing using videometric techniques. Int. Arch. Photogrammetry and Remote Sensing, Vol. 30 (5), pp 41-46.
- El-Hakim, S. F., 1992. Application and performance evaluation of a vision-based automated measurement system. Videometrics, SPIE Vol. 1820, pp 181-195.
- Fraser, C. S., 1986. Microwave antenna measurement by photogrammetry. Photogrammetric Engineering and Remote Sensing, 52 (10) : 1627-1635.
- Fraser, C. S. and Shortis, M. R., 1995. Metric exploitation of still video imagery. The Photogrammetric Record, 15(85) : 107-122.
- Fryer, J. G. and Mason, S. O., 1989. Rapid lens calibration of a video camera. Photogrammetric Engineering and Remote Sensing, 55(4) : 437-442.
- Gustafson, P. C. and Handley, H. B., 1992. A video-based industrial measurement system. Int. Arch. Photogrammetry and Remote Sensing, Vol. 28(5): 501-506.

- Hentschel, M. J. and Shortis, M. R., 1991. Calibration of cameras under operational conditions. The Australian Surveyor, 36(1) : 61-74.
- Haggrén, H. and Leikas, E., 1987. Mapvision: The photogrammetric machine vision system. Photogrammetric Engineering and Remote Sensing, 53(8):1103-1108.
- Maas, H-G., 1991. Digital photogrammetry for determination of tracer particle coordinates in turbulent flow research. Photogrammetric Engineering and Remote Sensing, 57(12):1593-1597.
- Maas, H-G., 1992. High-speed solid state camera systems for digital photogrammetry. Int. Arch. Photogrammetry and Remote Sensing, Vol. 28(5): 482-485.
- Shortis, M. R., 1989. Industrial photogrammetry at the NASA Langley Research Center. Proceedings, Symposium on Surveillance and Monitoring Surveys, University of Melbourne, Australia, pp 218-231.
- Shortis, M. R., Clarke, T. A. and Short, T., 1994. A comparison of some techniques for the subpixel location of discrete target images. Videometrics III, SPIE Vol. 2350, pp 239-250.
- Shortis, M. R. and Hall, C. J., 1989. Network design methods for close range photogrammetry. Australian Journal of Geodesy, Photogrammetry and Surveying 50 : 51-72.
- Shortis, M. R., Burner, A. W., Snow, W. L., and Goad, W. K., 1991. Calibration tests of industrial and scientific CCD cameras. Invited paper (Paper 6, Volume 1), First Australian Photogrammetric Conference, Sydney, Australia, 11 pages.
- Shortis, M. R., Snow, W. L. and Goad, W. K., 1995. Comparative geometric tests of industrial and scientific CCD cameras using plumb line and test range calibrations. Proceedings, ISPRS Intercommission Workshop "From Pixels to Sequences", Zurich, Switzerland, pp 53-59.
- Snow, W. L., Childers, B. A., Jones, S. B. and Fremaux, C. M., 1992. Recent experiences with implementing a video based six degrees of freedom measurement system for airplane models in a 20 foot diameter vertical spin tunnel. Videometrics, SPIE Vol. 1820, pp 158-180.
- Trinder, J. C., 1989. Precision of digital target location. Photogrammetric Engineering and Remote Sensing, 55 (6) : 883-886.
- Wiley, A. G. and Wong, K. W., 1995. Geometric calibration of zoom lenses for computer vision metrology. Photogrammetric Engineering and Remote Sensing, 61 (1) : 69-74.